Quantized Compressive Sensing for Low-Power Data Compression and Wireless Telemonitoring

Benyuan Liu and Zhilin Zhang

***Abstract*— In low-power wireless telemonitoring, physiological signals must be compressed before transmission to extend battery life. In this paper, we propose a two-stage data compressor based on quantized compressive sensing (QCS), where signals are first compressed by compressive sensing with a 50% compression ratio and then quantized with 2 bits per measurement. We also develop a reconstruction algorithm, called Bayesian dequantization (BDQ), to recover signals from the quantized compressed measurements. This algorithm exploits both the model of quantization errors and the correlated structure of physiological signals, which improves the quality of recovery. We validate the proposed data compressor and the recovery algorithm on wrist-type photoplethysmography data. This data are used to estimate the heart rate during fitness training. Results show that an average estimation error of 2.596 beats per minute is achieved using QCS and BDQ. This accuracy approaches the performance on non-compressed data, but we transmit *n* bits instead of *n* samples, which is a substantial improvement for low-power telemonitoring.**

***Index Terms*— Quantized compressive sensing, block sparse Bayesian learning, data compression, telemonitoring.**

I. Introduction

In WIRELESS health monitoring [1], hybrid types of physiological signals are collected from on-body sensors, then these data are transmitted to nearby smart phones or a data central via wireless networks. The wearable devices are usually battery powered. To reduce the power consumption and extend battery life, data must be compressed before transmission.

Compressive sensing (CS) [2] is an emerging technique for low-power data compression and wireless transmission [3], [4]. In CS, a signal $\mathbf{x}$ of length N is compressed by a simple matrix-vector multiplication,

$$\mathbf{y} = \mathbf{\Phi x} \tag{1}$$

where $\mathbf{\Phi} \in \mathbb{R}^{M\times N}$ is the sensing matrix and $\mathbf{y} \in \mathbb{R}^{M}$ is the compressed measurements. Usually $\mathbf{\Phi}$ is underdetermined and $(N-M)/N$ is called the compression ratio (CR) of CS. At the receiver, signals are reconstructed from compressed measurements via CS solvers [2], [5].

Manuscript received March 1, 2016; accepted March 25, 2016. Date of publication April 5, 2016; date of current version November 4, 2016. The associate editor coordinating the review of this paper and approving it for publication was Prof. Zeljko Ignjatovic.

B. Liu is with the Department of Biomedical Engineering, Fourth Military Medical University, Xi'an 710032, China (e-mail: byliu@fmmu.edu.cn).

Z. Zhang is with Samsung Research America–Dallas, Richardson, TX 75082 USA (e-mail: zhilinzhang@ieee.org).

Digital Object Identifier 10.1109/JSEN.2016.2550602

The merit of the CS-based data compressor is its low-power, low-complexity properties [6]. It can be implemented using analog circuitry [7] or digitally in MCU [6] or FPGA [8]. CS has been successfully used in low-power telemonitoring of physiological signals such as Electroencephalogram (EEG) [9] and fetal Electrocardiogram (fECG) [3].

However, existing works [3], [9] assumed that the compressed measurement $\mathbf{y}$ was real-valued with infinite precision. In practice, $\mathbf{y}$ must be quantized before transmission, i.e.,

$$\mathbf{z} = \mathcal{Q}(\mathbf{y}), \quad \mathbf{y} = \mathbf{\Phi x} \tag{2}$$

where $\mathcal{Q}(\cdot)$ is a quantization operator that maps a real-value to finite quantization levels [10].

Quantization inevitably introduces errors. But suitably using quantization can largely reduce the wireless transmission bit-budget [11]. Quantized CS (QCS) is attractive for power or bandwidth limited telemonitoring applications and various algorithms [12], [13] were developed to recover signals from quantized measurements. In this architecture, the recovery procedure is called de-quantization [14] and a CS recovery algorithm is called a decoder [15]. Haboba *et al.* [16] studied the quantization error and its effect on signal recovery. However, they used synthetic signals with fixed sparsity, which is not practical for telemonitoring applications, as most physiological signals are only approximately sparse. Wang *et al.* [17], [18] were the first to use QCS in low-energy telemonitoring of EEG signals. But the CS algorithm used in [17] ignored the model of quantization error, which may yield degraded performance.

In this work, we use quantized CS for low-power telemonitoring. First, physiological signals are compressed according to (1), and then quantized according to (2). The model of QCS is presented in Section II.

In Section III, we propose a Bayesian de-quantization algorithm, called BDQ. It exploits both the correlated structure within physiological signals and the model of quantization error. Note that this algorithm does not exploit sparsity to recover signals, as done by most other compressive sensing algorithms. Instead, it only exploits correlation of physiological signals, which is an alternate way of using the temporal smooth structure of signals such as in the Block Sparse Bayesian Learning (BSBL) framework [3]. However, BSBL [3] did not consider quantization errors, and thus has inferior performance to BDQ, as shown in experiments later.

In Section IV, we study the application of telemonitoring for fitness training, in which photoplethysmography (PPG)

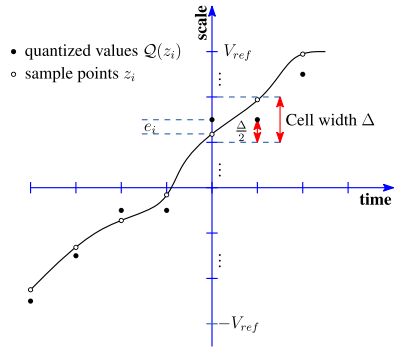

Fig. 1. Time sampling and scale quantization. The quantization error is denoted by e_i and the cell width is Δ. The mid-point value within a cell is taken as the quantized value for a sample point falling in that cell.

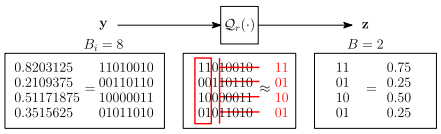

Fig. 2. The operator $\mathcal{Q}_r(\cdot)$ can be efficiently implemented in digital CS. In this example, the compressed measurements $\mathbf{y}$ are represented using unsigned fix-point arithmetic ($B_i = 8$ and the fraction length is 8 bits). The rounding outputs $\mathbf{z}$ have only 2-bit per sample.

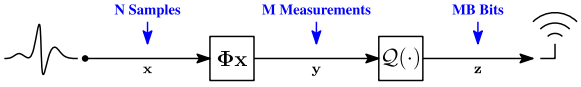

Fig. 3. A unified framework for low-power wireless telemonitoring using quantized compressed sensing.

and accelerometer signals are transmitted and used to estimate the heart rate during intensive physical exercises. We exploit the optimum compression by jointly tuning the compression ratio (CR) of CS and the quantization bit-depth. Results show that an average absolute heart rate estimation error of 2.596 BPM is achieved with CR = 0.50 and a 2-bit quantizer. The heart rate estimation accuracy approaches the state-of-the-art on non-compressed data [19]. These findings imply that we can compress segments of PPG and accelerometer data from n samples to n bits for low-power telemonitoring.

II. The Model of Quantized CS

A. Quantization

The function of an ADC is *time* sampling and *scale* quantization, which is illustrated in Fig 1.

Let B denotes the number of bits per measurement, which is also called the bit-depth of a quantizer. Represented by B bits, the scales between the positive and negative reference voltage $[-V_{ref}, V_{ref}]$ are divided into $L = 2^B$ quantization levels. The cell width [10] Δ of a uniform quantizer is

$$\Delta = \frac{2V_{ref}}{2^B}. \tag{3}$$

Signals larger than V_{ref} or smaller than $-V_{ref}$ are saturated. Those saturation signals are quantized with the same level as signals in $[V_{ref} - \Delta, V_{ref}]$ or $[-V_{ref} + \Delta, -V_{ref}]$.

For a sample $v_i \in \mathbb{R}$ falls in a cell, the mid-point value in that cell is used as the quantization value $\mathcal{Q}(v_i)$. The quantization error e_i is,

$$e_i = \mathcal{Q}(v_i) - v_i, \tag{4}$$

e_i distributes uniformly between $[-\Delta/2, \Delta/2]$. The variance of the quantization error, denoted by σ_e, is

$$\sigma_e = \frac{\Delta^2}{12}. \tag{5}$$

Note that the sampling process for PPG or accelerometer signals is non-coherent and the quantization error is assumed uniform. In practice, the quantization error may depend on the amplitude or frequency of the signal. Exploiting such information might improve the reconstruction results. However, this relationship is inherently non-uniform and non-exact, which is hard to incorporate into the Bayesian model [13].

B. Data Compression via QCS

In CS-based data compressor, analog signals are firstly quantized by an ADC via Nyquist sampling, then these digitized samples are compressed by a simple matrix-vector multiplication,

$$\mathbf{y} = \mathbf{\Phi}\mathbf{x}_q + \mathbf{n}, \quad \mathbf{x}_q = \mathcal{Q}(\mathbf{x}), \tag{6}$$

where $\mathbf{n}$ is the measurement noise.

In practice, larger bit-depth B_i is required to reduce the distortions during signal acquisition (i.e., $B_i = 12$ was used in [8]). For larger B_i, the variance of the quantization error $\mathbf{e}$ is smaller and (6) can be simplified as,

$$\mathbf{y} = \mathbf{\Phi}\mathbf{x}_q + \mathbf{n}, \quad \mathbf{x}_q \approx \mathbf{x} \tag{7}$$

In (6), both $\mathbf{y}$ and $\mathbf{x}_q$ are represented using fixed-point arithmetic with B_i bits. We may further reduce the transmission bit-budget by simply rounding each sample to B bits, denoted by $\mathbf{z} = \mathcal{Q}_r(\mathbf{y})$, where $\mathcal{Q}_r(\cdot)$ is a rounding operator and its function is illustrated in Fig 2. $\mathcal{Q}_r$ is in fact an economy quantizer using fixed-point arithmetic.

We denote by $\mathbf{e}_r = \mathbf{z} - \mathbf{y}$ the rounding error, which is assumed to be uniform distributed,

$$p(e_r) \sim \mathcal{U}(\mathcal{D}_{e_r}) \tag{8}$$

where $\mathcal{D}_{e_r} \triangleq [-\Delta_r/2, \Delta_r/2]$ and the cell width $\Delta_r = \frac{2V_{ref}}{2^B}$.

After rounding, (7) can be reformulated as,

$$\mathbf{z} = \mathbf{\Phi}\mathbf{x}_q + \mathbf{e} + \mathbf{n}, \quad \mathbf{x}_q \approx \mathbf{x}. \tag{9}$$

The use of QCS in low-energy telemonitoring is shown in Fig 3, where $\mathbf{z}$ is the quantized measurement represented with B bits per sample, $\mathbf{\Phi} \in \mathbb{R}^{M \times N}$ is the sensing matrix, $\mathbf{n}$ and $\mathbf{e}$ are measurement noise and quantization noise respectively. In this framework, we transmit MB bits instead of N samples for wireless telemonitoring.

III. The Bayesian DeQuantize Algorithm

A. Bayesian Hierarchical Model

1) Noise Model: The measurement noise $\mathbf{n}$ is usually assumed Gaussian with variance λ, i.e., $\mathbf{n} \sim \mathcal{N}(\mathbf{0}, \lambda\mathbf{I})$. From (9) we have,

$$p(\mathbf{z}|\mathbf{x}, \mathbf{e}; \lambda) = \mathcal{N}(\mathbf{\Phi}\mathbf{x} + \mathbf{e}, \lambda\mathbf{I}). \tag{10}$$

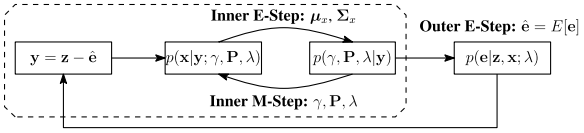

Fig. 4. Bayesian dequantization algorithm using nested EM approach.

The quantization error $\mathbf{e}$ is uniform distributed,

$$p(\mathbf{e}) = \mathcal{U}(\mathcal{D}_e) \tag{11}$$

where $\mathcal{D}_e \triangleq [-\Delta/2, \Delta/2]$ and $\Delta = \frac{2V_{ref}}{2^B}$.

Remark 1: We only study multi-bit ($B \geq 2$) QCS and do not consider the extreme case such as 1-bit compressed sensing. 1-bit CS may have better recovery performance than multi-bit CS with the same compressed bit-budget MB [12]. However, 1-bit CS loses the scale information of signals, which limits its use in low-power telemonitoring applications.

2) Signal Model: We assume a correlated structure within signals [5], the prior of $\mathbf{x}$ is,

$$p(\mathbf{x}|\gamma, \mathbf{P}) = \mathcal{N}(\mathbf{0}, \gamma\,\mathbf{P}) \tag{12}$$

where γ is a non-negative parameter controlling the variance of $\mathbf{x}$, $\mathbf{P}$ is a symmetric positive semi-definite matrix modeling the correlation structure of signals.

B. The Bayesian Dequantization Algorithm

We estimate $\{\mathbf{x}, \mathbf{e}, \lambda, \gamma, \mathbf{P}\}$ using their joint MAP estimator,

$$\begin{aligned}\{\hat{\mathbf{x}}, \hat{\mathbf{e}}, \hat{\lambda}, \hat{\gamma}, \hat{\mathbf{P}}\} &= \arg\max \log p(\mathbf{x}, \mathbf{e}, \lambda, \gamma, \mathbf{P}|\mathbf{z}) \\ &= \arg\max \log p(\mathbf{e}|\mathbf{z}, \mathbf{x}, \lambda, \gamma, \mathbf{P}) \cdot p(\mathbf{x}, \lambda, \gamma, \mathbf{P}|\mathbf{z}).\end{aligned}$$

A nested Expectation Maximization (nest-EM) approach [20] is adopted. The nest-EM is consisted of an inner and outer EM loop, which is briefly sketched in Fig 4.

We initialized the nest-EM procedure with $\mathbf{e}_0 = \mathbf{0}$ and $\mathbf{y} = \mathbf{z} - \mathbf{e}_0$, then iterative over

- **Inner E-Step**, estimate $\boldsymbol{\mu}_x$ and $\boldsymbol{\Sigma}_x$ from posterior probability $p(\mathbf{x}|\mathbf{y}; \gamma, \mathbf{P}, \lambda)$,
- **Inner M-Step**, update γ, $\mathbf{P}$ and λ via maximize the likelihood $p(\gamma, \mathbf{P}, \lambda|\mathbf{y})$,
- **Outer E-Step**, estimate the first moment of quantization error $\hat{\mathbf{e}}$ from $p(\mathbf{e}|\mathbf{z}, \mathbf{x}; \lambda)$, and update $\mathbf{y} = \mathbf{z} - \hat{\mathbf{e}}$.

1) Inner-E Step: The posterior $p(\mathbf{x}|\mathbf{y}; \lambda, \gamma, \mathbf{P})$ can be expressed in an analytic form,

$$\begin{aligned}p(\mathbf{x}|\mathbf{y}; \lambda, \gamma, \mathbf{P}) &= \frac{p(\mathbf{y}|\mathbf{x}; \lambda)\, p(\mathbf{x}|\gamma, \mathbf{P})}{p(\mathbf{y}|\lambda, \gamma, \mathbf{P})} \\ &= (2\pi)^{-(N+1)/2} |\boldsymbol{\Sigma}|^{-1/2} \exp\left\{-\frac{1}{2}(\mathbf{x} - \boldsymbol{\mu})^T \boldsymbol{\Sigma}^{-1} (\mathbf{x} - \boldsymbol{\mu})\right\},\end{aligned}$$

where $\boldsymbol{\mu}$ and $\boldsymbol{\Sigma}$ are,

$$\boldsymbol{\mu} = \gamma\,\mathbf{P}\boldsymbol{\Phi}^T (\lambda\mathbf{I} + \gamma\,\boldsymbol{\Phi}\mathbf{P}\boldsymbol{\Phi}^T)^{-1}\mathbf{y} \tag{13}$$

$$\boldsymbol{\Sigma} = (\frac{1}{\gamma}\mathbf{P}^{-1} + \frac{1}{\lambda}\boldsymbol{\Phi}^T\boldsymbol{\Phi})^{-1} \tag{14}$$

2) Inner-M Step: The parameters λ, γ and $\mathbf{P}$ are estimated by a Type-II maximum likelihood procedure,

$$\mathcal{L}(\lambda, \gamma, \mathbf{P}) = -\log p(\mathbf{y}|\lambda, \gamma, \mathbf{P}) \tag{15}$$

$$= \log|\lambda\mathbf{I} + \gamma\,\boldsymbol{\Phi}\mathbf{P}\boldsymbol{\Phi}^T| + \mathbf{y}^T \left(\lambda\mathbf{I} + \gamma\,\boldsymbol{\Phi}\mathbf{P}\boldsymbol{\Phi}^T\right)^{-1}\mathbf{y} \tag{16}$$

Optimize over $\mathcal{L}(\lambda, \gamma, \mathbf{P})$, we have,

$$\lambda = \frac{\|\mathbf{y} - \boldsymbol{\Phi}\boldsymbol{\mu}\|_2^2 + \mathrm{Tr}(\boldsymbol{\Sigma}\boldsymbol{\Phi}^T\boldsymbol{\Phi})}{M} \tag{17}$$

$$\mathbf{P} = \frac{\boldsymbol{\Sigma} + \boldsymbol{\mu}\boldsymbol{\mu}^T}{\gamma} \tag{18}$$

$$\gamma = \frac{1}{N}\mathrm{Tr}\left[\mathbf{P}^{-1}(\boldsymbol{\Sigma} + \boldsymbol{\mu}\boldsymbol{\mu}^T)\right]. \tag{19}$$

Remark 2: Due to the coupling of $\mathbf{e}$ and $\mathbf{n}$ in (9), the estimate of the noise variance λ is inaccurate due to an identifiability issue as stated in [21]. Therefore, λ is often treated as a regularization parameter [8], [13]. We set $\lambda = 0.001$ as the default parameter in the experiment.

3) Regularization on P: Regularization on $\mathbf{P}$ is required due to limited data. Zhang and Rao [5] provided an empirical method on the regularization of $\mathbf{P}$ using a symmetric Toeplitz matrix,

$$\mathbf{P}_{ij} = r^{|i-j|}, \qquad i, j = 1, \cdots, N, \quad |r| < 1 \tag{20}$$

where r is the correlation coefficient empirically calculated from the ratio between the mean of sub-diagonal of $\mathbf{P}$ and the mean of main diagonal of $\mathbf{P}$. Such regularization is equivalent to modeling the correlation structure as a first-order Auto-Regressive (AR) process [21].

An AR(1) matrix has simple tri-diagonal inverse,

$$\mathbf{P}^{-1} = \frac{1}{1-r^2}\begin{pmatrix} 1 & -r & 0 & \cdots & 0 \\ -r & 1+r^2 & -r & \cdots & 0 \\ \vdots & \ddots & \ddots & \ddots & \vdots \\ 0 & \cdots & -r & 1+r^2 & -r \\ 0 & \cdots & 0 & -r & 1 \end{pmatrix} \tag{21}$$

and it can be decomposed as

$$\mathbf{P}^{-1} = \frac{1}{1-r^2}\mathbf{T}\left(\mathbf{D}^T\mathbf{D}\right) \tag{22}$$

where $\mathbf{T} = \mathrm{diag}\{1, \cdots, 1, 1/(1+r^2)\}$ is a diagonal matrix and $\mathbf{D}$ is a temporal smooth operator defined as,

$$\mathbf{D} = \begin{pmatrix} 1 & -r & 0 & \cdots & 0 \\ 0 & 1 & -r & \cdots & 0 \\ & \ddots & \ddots & \ddots & \\ 0 & 0 & \cdots & 1 & -r \\ 0 & 0 & \cdots & 0 & 1 \end{pmatrix}. \tag{23}$$

A similar regularization method was proposed in [22] which models the inverse covariance matrix as $\mathbf{D}^T\mathbf{D}$.

The AR(1) matrix models the correlated structures within physiological signals [3], [9]. However, the correlation coefficient r in (20) or (23) can only be empirically calculated [5] or fixed [22] in existing algorithms.

We present an AR(1) approximation method to estimate the correlation matrix in (18) using Karhunen-Loeve Transform (KLT) [23]. The correlation matrix $\mathbf{P}$ calculated by (18) is a symmetric, positive semi-definite matrix. Let

$$\mathbf{U}\mathbf{D}\mathbf{U}^T = \text{SVD}(\mathbf{P}) \tag{24}$$

denotes the Singular Value Decomposition (SVD) of $\mathbf{P}$, where columns of $\mathbf{U}$ are the eigenvectors of $\mathbf{P}$ and $\mathbf{D}$ is a diagonal matrix with diag($\mathbf{D}$) being descending ordered eigenvalues of $\mathbf{P}$. It has been shown in [24] that the basis vectors of a Discrete Cosine Transform (DCT) approach to the eigenvectors of the inverse of an AR(1) matrix as the coefficient r goes to 1. This property of DCT has made it a popular transform for decomposition of highly correlated signals [23].

From (18) and (24), we can regularize the correlation matrix $\mathbf{P}$ with an AR(1) matrix by simply substituting the eigenvalue matrix $\mathbf{U}$ in (24) with a DCT Type-2 matrix,

$$\tilde{\mathbf{P}} = \text{dctmtx}(N)^T\, \mathbf{D}\, \text{dctmtx}(N) \tag{25}$$

where dctmtx(N) generates a DCT Type-2 matrix of size N. Then, the diagonal entries of $\tilde{\mathbf{P}}$ are normalized to 1s by

$$\mathbf{v} = \sqrt{\text{diag}(\tilde{\mathbf{P}})}, \quad \bar{\mathbf{P}} = \text{diag}^{-1}(\mathbf{v})\tilde{\mathbf{P}}\text{diag}^{-1}(\mathbf{v}) \tag{26}$$

where $\text{diag}^{-1}(\mathbf{v})$ builds a diagonal matrix with the diagonal entries given by $\mathbf{v}$. In (26), $\bar{\mathbf{P}}$ is the AR(1) approximation to the correlation matrix $\mathbf{P}$.

γ is updated afterwards using the regularized $\bar{\mathbf{P}}$,

$$\gamma = \frac{1}{N}\text{Tr}\left[\bar{\mathbf{P}}^{-1}(\boldsymbol{\Sigma} + \boldsymbol{\mu}\boldsymbol{\mu}^T)\right]. \tag{27}$$

Remark 3: Using KLT to exploit the correlation structure in signals has long been exist in the literature. In [23], the author used Toeplitz matrix to approximate empirical correlation matrix. To our best knowledge, our work is the first to use KLT in regularized least squares to solve underdetermined optimization problems. The DCT approximation in (25) is also attractive for its computational efficiency in calculating $\boldsymbol{\mu}$, $\boldsymbol{\Sigma}$ and γ in (13), (14) and (27).

4) Estimate the Quantization Error $\mathbf{e}$ (Outer-E Step): We calculate the expected value of $\mathbf{e}$ from

$$\hat{\mathbf{e}} = E[\mathbf{e}|\mathbf{e} \in \mathcal{D}_e] = \int_{-\Delta/2}^{\Delta/2} \mathbf{e}\; p(\mathbf{e}|\mathbf{z}, \mathbf{x}; \lambda)\text{d}\mathbf{e}$$

which is the expected value of a truncated Normal distribution. $\hat{\mathbf{e}}$ can be obtained analytically [13] by,

$$\hat{\mathbf{e}} = \boldsymbol{\mu}_e - \sqrt{\lambda} \cdot \frac{\text{PDF}(\mathbf{l}_e) - \text{PDF}(\mathbf{u}_e)}{\text{CDF}(\mathbf{l}_e) - \text{CDF}(\mathbf{u}_e)} \tag{28}$$

where $\boldsymbol{\mu}_e = \mathbf{z} - \boldsymbol{\Phi}\boldsymbol{\mu}_x$, $\mathbf{l}_e = (-\Delta/2 - \boldsymbol{\mu}_e)/\sqrt{\lambda}$ and $\mathbf{u}_e = (\Delta/2 - \boldsymbol{\mu}_e)/\sqrt{\lambda}$. PDF($\cdot$) and CDF($\cdot$) are the probability density function (PDF) and cumulative density function (CDF) of a standard Normal distribution respectively.

procedure BDQ($\mathbf{z}$,$\boldsymbol{\Phi}$)
  Outputs: $\mathbf{x}, \mathbf{e}$
  Initialize: $\gamma = 1$, $\mathbf{P} = \mathbf{I}$, $\lambda = 0.001$
  while not converged **do**
    Estimate $\boldsymbol{\mu}$, $\boldsymbol{\Sigma}$ by (13), (14).
    Calculate $\mathbf{P}$ via (18)
    Regularize $\bar{\mathbf{P}}$ via (25)-(26).
    Calculate γ via (27).
    Calculate $\hat{\mathbf{e}}$ by (28)
    Update $\mathbf{y} = \mathbf{z} - \hat{\mathbf{e}}$
  end while
end procedure

Fig. 5. The Bayesian dequantize (BDQ) algorithm.

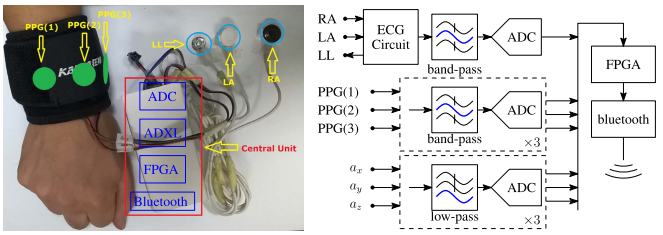

Fig. 6. The hardware setup for data recording. ECG, PPG and accelerometer signals were simultaneously collected. Wet electrodes were used to obtain a three-lead ECG, where the leads LA and RA were placed at left and right chest, respectively, and the LL lead was placed at the left lower abdomen. PPG signals were collected using reflective pulse oximeter sensors with green LED (wavelength: 515nm). Two PPG sensors were placed at the back of the wrist while another one was placed right on the pulse position. Three axial accelerometer data were collected using ADXL345 with ±4g range. Data were transmitted to a laptop via Bluetooth.

5) The Proposed Algorithm: The resulting algorithm is summarized in Fig 5, named as the Bayesian De-Quantize algorithm (**BDQ**).

Remark 4: The **BDQ** algorithm can be used to recover piecewise smooth signals from quantized, and possibly underdetermined measurements. It shares some similarities with the Block Sparse Bayesian Learning (BSBL) framework [5] where only the correlations within signals are exploited. However in the experiment, we find that the regularization method (25)-(26) on $\mathbf{P}$ in **BDQ** is superior to the empirical methods in BSBL, which yields better recovery results.

IV. Experiments and Results

A. Datasets

We simultaneously collected ECG, PPG and accelerometer signals from 12 volunteers with age ranged from 18 to 35. Fig 6 shows the hardware setup for data recording.

For each subject, we recorded data for 5 $\sim$ 6 minutes. During data collection, a subject ran on a treadmill with speeds ranged from 2km/hour to 15km/hour. The sensor band was conveniently worn on the wrist and we intentionally introduced additional artifacts by asking all subjects to pull clothes, wipe sweat, swig arms during data recording.

All signals were filtered and then sampled at 125Hz with 12 bits precision per sample. Table I shows the specifications for all analog filters.

TABLE I

SPECIFICATIONS FOR ANALOG FILTERS. f_{c1} AND f_{c2} DENOTE THE LOWER AND UPPER CUTOFF FREQUENCIES AT 22dB ATTENUATION

	ECG	PPG	Accelerometer
Filter Type	Band-pass	Band-pass	Low-pass
f_{c1}	0.1Hz	0.25Hz	–
f_{c2}	100Hz	14.5Hz	100Hz

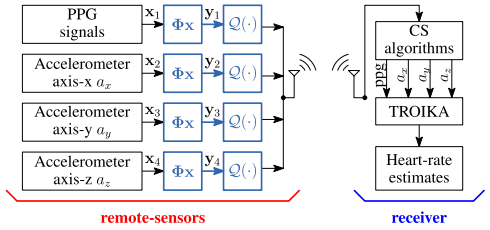

Fig. 7. The quantized compressed sensing is applied on PPG and three axial accelerometer data to reduce the transmission bit-budget. At the receiver, data are recovered from quantized measurements, and we use the TROIKA framework to estimate heart rates from the recovered data.

In the experiment, ECG signals were used as reference signals to extract the ground truth heart rates. The TROIKA [19] framework was used to estimate the heart rates from wrist type PPG signals during physical exercises. It should be noted that three-axis accelerometer data were also used by TROIKA to remove movement artifacts. We down-sampled PPG and accelerometer signals to 31.75Hz. The accelerometer data may alias when sampled at 31.75Hz. However, such distortions were small as the rate of most activities during fitness training rarely exceeded 10Hz.

B. Experiments Setup

Fig 7 shows the experiment setup. Quantized compressed sensing is applied on PPG and accelerometer signals. Raw segments $\{\mathbf{x}_1, \mathbf{x}_2, \mathbf{x}_3, \mathbf{x}_4\}$ from each data channel are compressed by $\mathbf{y}_i = \mathbf{\Phi}\mathbf{x}_i$ simultaneously. Sparse binary sensing matrices, whose entries consisted of only 0s and 1s, are used. We fix each column of $\mathbf{\Phi}$ consisting exactly 2 non-zero entries and also make sure $\mathbf{\Phi}$ is full row-rank. Such matrix supports on-the-fly compression [25] and consumes extremely low power when implemented in FPGA [8]. The compressed measurements $\{\mathbf{y}_1, \mathbf{y}_2, \mathbf{y}_3, \mathbf{y}_4\}$ are further quantized by $\mathcal{Q}(\cdot)$ to reduce the transmission bit-budget.

At the receiver, CS algorithms are used to recover signals from quantized measurements. The heart rate is estimated by TROIKA using the recovered data.

C. Performance Measurement

We use two performance metrics. One is the reconstruction SNR (RSNR),

$$\text{RSNR (dB)} = 10\log_{10}\frac{\|\mathbf{x}\|_2^2}{\|\hat{\mathbf{x}} - \mathbf{x}\|_2^2}$$

where $\hat{\mathbf{x}}$ denotes the recovered signal of $\mathbf{x}$. To assess the averaged performance over all segments, we refer to the average RSNR (ARSNR), defined by

$$\text{ARSNR (dB)} = 10\log_{10}\frac{1}{S}\sum_{i=1}^{S}\left(\frac{\|\mathbf{x}_i\|_2^2}{\|\hat{\mathbf{x}}_i - \mathbf{x}_i\|_2^2}\right) \tag{29}$$

where $\mathbf{x}_i$ is the ith signal segment and S is the total number of segments. The second metric is the Structural SIMilarity index (SSIM) [26]. SSIM measures the similarity between recovered signals and original signals, which is a better metric than RSNR [9], [26].

The qualities of recovery are not only characterized by RSNR or SSIM, but also by application specific requirements. Therefore, we estimate heart rates from the recovered PPG and accelerometer signals. The average absolute estimation error (Error1), defined in [19], is

$$\text{Error1} = \frac{1}{W}\sum_{i=1}^{W}|\text{BMP}_{\text{est}}(i) - \text{BPM}_{\text{true}}(i)| \tag{30}$$

where W is the total number of heart rate estimates, $\text{BPM}_{\text{est}}(i)$ is the estimated heart rate in the ith time window[1] and $\text{BPM}_{\text{true}}(i)$ is the ground truth heart rate. The standard deviation of heart rate estimates, denoted by SD_{BPM}, is

$$\text{SD}_{\text{BPM}} = \sqrt{\frac{1}{W}\sum_{i=1}^{W}(\text{BMP}_{\text{est}}(i) - \text{BPM}_{\text{true}}(i))^2} \tag{31}$$

Pearson correlation between the ground-truth and the estimates is also calculated for comparison.

D. Recovery Algorithms for Quantized CS

We compared the proposed algorithm with the following two CS algorithms: QVMP [13] and BSBL-BO [3].

1) QVMP [13]: QVMP is a variational Bayesian De-Quantization algorithm proposed in [13]. It has better performance than QIHT [12] and L1RML [27]. However, QVMP can not recover physiological signals directly in time domain. Instead, we applied QVMP in a transformed domain, where

$$\mathbf{z} = (\mathbf{\Phi}\mathbf{\Psi})\boldsymbol{\theta} + \mathbf{e} + \mathbf{n}$$

$\mathbf{\Psi}$ is a sparse representation matrix and $\boldsymbol{\theta}$ is the sparse coefficients. QVMP firstly recovered $\hat{\boldsymbol{\theta}}$, then $\hat{\mathbf{x}}$ via $\hat{\mathbf{x}} = \mathbf{\Psi}\hat{\boldsymbol{\theta}}$.

In the experiment, Discrete Cosine Transform (DCT) matrix was selected for $\mathbf{\Psi}$ and we set $\lambda = 0.001/M$, tol $= 1e^{-6}$, maxiter $= 400$ for QVMP as it achieved the best recovery performance on the dataset.

2) BSBL-BO [5]: BSBL is currently the state-of-the-art algorithm in recovering physiological signals such as fetal ECG [3] or EEG [9]. In the experiment, we observed that BSBL-BO can also recover signals from quantized measurements, by modeling quantization errors using a zero mean Normal distribution with a larger variance λ_e.

Throughout the experiment, BSBL-BO worked in non-sparse mode and directly recovered signals in time domain

[1]The TROIKA algorithm [19] operates in a sliding window manner. A time window of T seconds is sliding on the signals with incremental step S seconds. We use the default parameters ($T = 8$s, $S = 2$s) for TROIKA in our experiments.

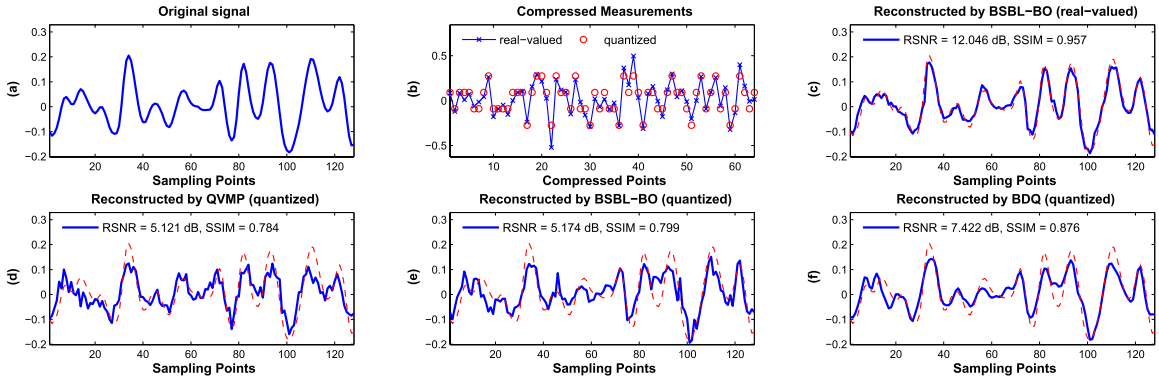

Fig. 8. Performances of different CS algorithms on quantized measurements. (a) A raw PPG segment $\mathbf{x}$ was collected ($N = 128$). (b) Real-valued compressed measurements ($M = 64$, CR $= 0.50$) were generated via $\mathbf{y} = \mathbf{\Phi x}$ and then quantized by $\mathcal{Q}(\cdot)$ with 2-bit per measurement. The transmission bit-budget was $MB = 128$ bits. (c) On real-valued measurements, BSBL-BO recovered original signals with RSNR $= 12.046$ dB and SSIM $= 0.957$. (d) QVMP recovered signals in DCT domain with RSNR $= 5.121$ dB and SSIM $= 0.784$. (e) and (f) BSBL-BO and BDQ recovered signals directly in time domain with RSNR $= 5.174$ dB, SSIM $= 0.799$ and RSNR $= 7.422$ dB, and SSIM $= 0.876$, respectively.

without resorting to any sparse representation matrix. We set blkLen $= 32$, LearnLambda $= 2$, maxiter $= 64$ and LearnType $= 1$ for BSBL-BO, as this setting achieved the best recovery performance. The recoveries of BSBL-BO using real-valued measurements were used as the benchmark, where LearnLambda $= 0$ was used.

E. Results

1) An Illustrative Example: To better understand quantized compressed sensing and the quality of signal recovery of different CS algorithms, we give an example in Fig 8.

1) Fig 8 (a), a raw PPG segment $\mathbf{x}$ of size $N = 128$. In the experiments, signals were divided into fix-sized segments and each segment was normalized (i.e., $\mathbf{x}/\|\mathbf{x}\|$) before compression.
2) Fig 8 (b), a segment $\mathbf{x}$ was compressed by $\mathbf{y} = \mathbf{\Phi x}$, where $\mathbf{\Phi}$ was a sparse binary matrix whose compression ratio CR $= 0.50$. $\mathbf{y}$ was further quantized by $\mathcal{Q}(\cdot)$ with $B = 2$ bits per measurement. The reference voltage of the quantizer was $V_{ref} = 0.70\max(\mathbf{y})$. The total transmission bit-budget was 128 bits.
3) Fig 8 (c) shows the recovery results using BSBL-BO with real-valued $\mathbf{y}$.
4) Fig 8 (d)(e)(f) show the recovery results using QVMP, BSBL-BO and BDQ with the quantized measurements $\mathbf{z} = \mathcal{Q}(\mathbf{y})$ respectively.

2) The Recovery Performances With Different Quantization Bit-Depth: Fig 9 shows the results using different quantization bit-depth $B \in \{2, 3, 4, 6, 8\}$. The proposed algorithm, BDQ, was in average 1.640dB superior to BSBL-BO and 3.547dB to QVMP.

For larger bit-depth such as $B \in \{6, 8\}$, the variance of the quantization error was small which can be approximated by a Normal distribution. However, in Fig 9, we observed a performance gap between BSBL-BO (real-valued) and BSBL-BO (quantized) when $B \in \{6, 8\}$. This may be caused by the saturation errors of the quantizer, whose distributions are unbounded and can not be approximated by a Normal distribution. In contrast, BDQ yielded similar recovery performance to BSBL-BO (real-valued) when $B \in \{6, 8\}$. The reasons were two-fold, one was that the regularization (25)-(26) on the correlation matrix can exploit the correlated structure in PPG signals, the other was that the learning rule (28) of quantization errors can account for mild saturation of the quantizer.

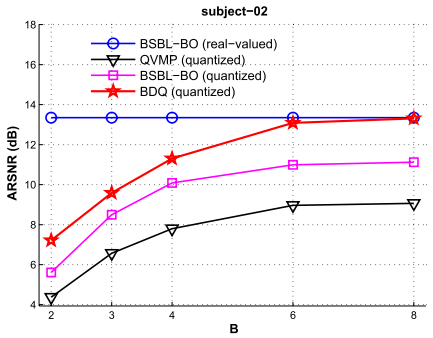

Fig. 9. The ARSNR in recovering PPG signals in dataset 'subject-02' with multiple quantization bit-depth B.

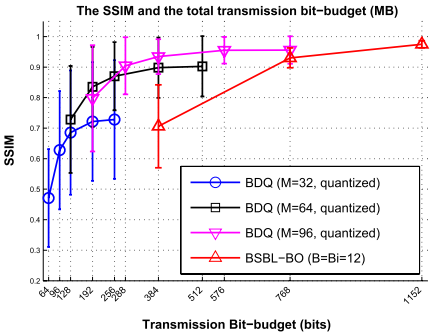

Fig. 10. The SSIM w.r.t different transmission bit-budget MB in recovering the PPG channel of dataset 'subject-02'. We fixed $N = 128$ and varied $M \in \{32, 64, 96\}$. BDQ was used to recover signals from quantized measurements with different bit-depth B.

3) The Trade-Off Between the Compression of CS and the Quantization Bit-Depth: Fig 10 shows the results with varying number of measurements $M \in \{32, 64, 96\}$ and quantization bit-depth $B \in \{2, 3, 4, 6, 8\}$. Fig 11 shows the absolute heart rate estimation error (Error1) and SD_{BPM} with respect to different transmission bit-budget.

In Fig 10 and Fig 11, we found that the qualities of recoveries were affected by the configurations of M and B

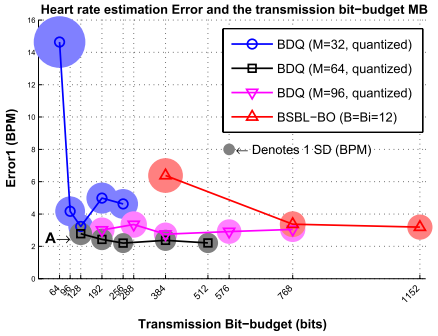

Fig. 11. The absolute heart rate estimation error (Error1) and $\mathrm{SD_{BPM}}$ w.r.t different transmission bit-budget MB. For each configuration (M, B), the diameter of a solid circle is proportional to the $\mathrm{SD_{BPM}}$ of this configuration. Point A denotes the default configuration of QCS where $M = 64$ and $B = 2$.

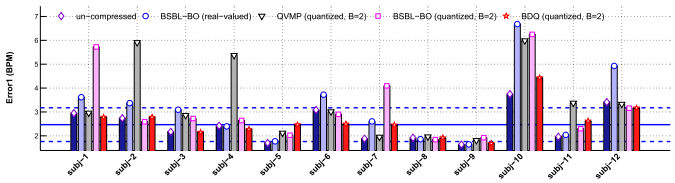

Fig. 12. The absolute heart rate estimation error (Error1) on each subject using non-compressed datasets (denoted by 'un-compressed') and the recovered datasets by different CS algorithms. The solid and the dashed line denote mean±standard deviation of Error1 using non-compressed datasets.

even if under the same transmission bit-budget MB. In fact, CS provides random mixing of signals to compressed measurements, each compressed measurement preserves information of original signals while quantization drops such information. It is worth noting that smaller values of MB is always preferable since it reduces the total transmission bit-budget. In Fig 11, the configuration $M = 64$ had the minimal Error1 for $MB < 512$ bits. We also found that $M = 64$, $B = 2$ yielded acceptable Error1 metric compared to the results using non-compressed data. This configuration has the minimal transmission bit budget, which will be used by QCS to compress PPG and accelerometer data.

With $M = 64$, $B = 2$, we may transmit 128 bits instead of 128 samples for low-power telemonitoring. Using an energy model of 0.4uJ/bit which facilitates Bluetooth Low-Energy (BLE) as the wireless transmission protocol [18], the energy consumption of QCS was 51.2uJ. For physiological signals quantized with B_i bits, the energy consumption of the QCS data compressor can be reduced to only $1/B_i$ of non-compressed telemonitoring.

4) Heart Rate Estimates From Recovered Datasets: We now presented results on whole datasets using the configurations $N = 128$, $M = 64$ (CR $= 0.50$) and $B = 2$ for QCS. Fig 12 shows the absolute error (Error1) per subject, Table II lists absolute error (Error1), Standard Deviation ($\mathrm{SD_{BPM}}$) and Pearson correlation. Using QCS and the proposed algorithm, we achieved $Error1 = 2.596$ (BPM), $\mathrm{SD_{BPM}} = 3.625$ (BPM) and 0.9899 Pearson correlation, which is close to the result using non-compressed data.

The Scatter Plot between the ground-truth heart rates and the estimates using the recovered datasets is shown in Fig 13. The fitted line for BSBL-BO and BDQ were $y = 0.999x - 0.866$, $(R^2 = 0.960)$ and $y = 1.002x - 1.333$, $(R^2 = 0.980)$ respectively, where x indicates the ground-truth heart rate and y is the estimate from recovered data, R^2 is a measure for goodness of linear fit.

TABLE II

AVERAGED ERROR1 AND THE PEARSON CORRELATION r OVER ALL 12 SUBJECTS USING THE DEFAULT CONFIGURATION OF QCS WHERE CR $= 0.50$, $B = 2$. NONE DENOTES THE RESULTS IN [19] USING NON-COMPRESSED DATA

	None	CS	QCS		
		BSBL-BO	QVMP	BSBL-BO	**BDQ**
Error1	**2.464**	3.137	3.355	3.179	**2.596**
$\mathrm{SD_{BPM}}$	**3.554**	5.022	5.561	5.030	**3.625**
r	**0.9902**	0.9810	0.9747	0.9798	**0.9899**

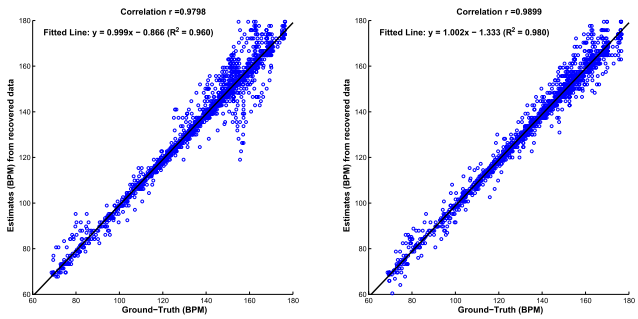

(a) (b)

Fig. 13. Scatter Plot between the ground-truth heart rates and the estimates using the recovered data by BSBL-BO (CR $= 0.50$, $B = 2$) and BDQ (CR $= 0.50$, $B = 2$). The Pearson correlation was 0.9798 and 0.9899 for BSBL-BO and BDQ respectively. The 'Fitted Line' is the linear fit of the estimates to ground-truth heart rates. The R^2 value, which is an estimate for goodness of linear fit, was 0.960 for BSBL-BO and 0.980 for BDQ. (a) BSBL-BO (CR $= 0.50$, $B = 2$). (b) BDQ (CR $= 0.50$, $B = 2$).

V. DISCUSSIONS

A. The Quantizer $\mathcal{Q}(\cdot)$

In our experiments, signal $\mathbf{x}$ was normalized via $\mathbf{x}/\|\mathbf{x}\|$ and then compressed by $\mathbf{y} = \mathbf{\Phi x}$, the reference voltage V_{ref} for the quantizer $\mathcal{Q}(\cdot)$ was fixed to $V_{ref} = 0.70 \max(\mathbf{y})$. Note that $V_{ref} = 0.70 \max(\mathbf{y})$ is not the optimal reference voltage for this dataset. Selecting the optimal reference voltage is out of the scope of this work, and is our future work.

At first sight, signal normalization $\mathbf{x}/\|\mathbf{x}\|$ and $\max(\mathbf{y})$ are not practical for implementing in hardware or for low power applications. This is usually solved by using an Automatic Gain Control (AGC) circuit to tune the scale of signals within $[-V_{ref}, V_{ref}]$. However, the gains of AGC must be transmitted with each compressed segments for signal recovery.

B. Signal Recovery Directly in the Time Domain

Most CS algorithms recover signals in a transform domain $\mathbf{\Psi}$ where signals $\mathbf{x}$ can be sparsely represented. By suitably choosing the transformation matrix, one may improve the quality of recovery.

However, physiological signals recorded by wearable devices are usually contaminated by various strong artifacts,

such as those due to body motion and hardware issues [28]. As a result, many of these signals are less sparse in many known transform domains. Seeking or designing an optimal transformation matrix for a specific kind of physiological signals may be difficult and recovering the signals from transform domains is not effective. In [3], BSBL-BO was used to recover raw fetal ECG recordings directly in the time domain by exploiting temporal correlations of these recordings, revealing that exploiting correlations of signals is an alternative method to exploiting sparsity. An obvious advantage of this method is that it avoids the seeking of an optimal transformation matrix for recovery. Our proposed BDQ algorithm also suggested the effectiveness of this method.

VI. Conclusions

In this paper, we present an approach for low-power wireless telemonitoring using quantized compressed sensing. The contributions of this paper are two-fold. First, we propose a two-stage data compressor based on QCS, which can effectively compress n samples down to n bits for transmission. Second, we develop a BDQ algorithm to recover signals from compressed measurements. Results showed that, by jointly using the proposed data compressor and the recovery algorithm, we achieved 2.596 heart rate estimation errors and 0.9899 Pearson correlation on whole datasets, which was close to the performance on non-compressed datasets. The data compressor proposed in this work is suitable for low-power wireless telemonitoring of physiological signals. It can also be used as a low-power data compressor or encoder for more types of signals such as audios and images.

Acknowledgment

The authors thank Dr. Hongqi Fan, Dr. Xiaoyi Pan for valuable discussions. They would also like to thank anonymous reviewers for providing insightful comments.

References

[1] C. A. Meier, M. C. Fitzgerald, and J. M. Smith, "eHealth: Extending, enhancing, and evolving health care," *Annu. Rev. Biomed. Eng.*, vol. 15, pp. 359–382, Jul. 2013.

[2] E. J. Candès and M. B. Wakin, "An introduction to compressive sampling," *IEEE Signal Process. Mag.*, vol. 25, no. 2, pp. 21–30, Mar. 2008.

[3] Z. Zhang, T.-P. Jung, S. Makeig, and B. D. Rao, "Compressed sensing for energy-efficient wireless telemonitoring of noninvasive fetal ECG via block sparse Bayesian learning," *IEEE Trans. Biomed. Eng.*, vol. 60, no. 2, pp. 300–309, Feb. 2013.

[4] D. Craven, B. McGinley, L. Kilmartin, M. Glavin, and E. Jones, "Compressed sensing for bioelectric signals: A review," *IEEE J. Biomed. Health Informatics*, vol. 19, no. 2, pp. 529–540, Mar. 2015.

[5] Z. Zhang and B. D. Rao, "Extension of SBL algorithms for the recovery of block sparse signals with intra-block correlation," *IEEE Trans. Signal Process.*, vol. 61, no. 8, pp. 2009–2015, Apr. 2013.

[6] H. Mamaghanian, N. Khaled, D. Atienza, and P. Vandergheynst, "Compressed sensing for real-time energy-efficient ECG compression on wireless body sensor nodes," *IEEE Trans. Biomed. Eng.*, vol. 58, no. 9, pp. 2456–2466, Sep. 2011.

[7] F. Chen, A. P. Chandrakasan, and V. M. Stojanovic, "Design and analysis of a hardware-efficient compressed sensing architecture for data compression in wireless sensors," *IEEE J. Solid-State Circuits*, vol. 47, no. 3, pp. 744–756, Mar. 2012.

[8] B. Liu, Z. Zhang, G. Xu, H. Fan, and Q. Fu, "Energy efficient telemonitoring of physiological signals via compressed sensing: A fast algorithm and power consumption evaluation," *Biomed. Signal Process. Control*, vol. 11, pp. 80–88, May 2014.

[9] Z. Zhang, T.-P. Jung, S. Makeig, and B. D. Rao, "Compressed sensing of EEG for wireless telemonitoring with low energy consumption and inexpensive hardware," *IEEE Trans. Biomed. Eng.*, vol. 60, no. 1, pp. 221–224, Jan. 2013.

[10] R. M. Gray and D. L. Neuhoff, "Quantization," *IEEE Trans. Inf. Theory*, vol. 44, no. 6, pp. 2325–2383, Oct. 1998.

[11] J. N. Laska, P. T. Boufounos, M. A. Davenport, and R. G. Baraniuk, "Democracy in action: Quantization, saturation, and compressive sensing," *Appl. Comput. Harmon. Anal.*, vol. 31, no. 3, pp. 429–443, 2011.

[12] L. Jacques, K. Degraux, and C. De Vleeschouwer, "Quantized iterative hard thresholding: Bridging 1-bit and high-resolution quantized compressed sensing," in *Proc. SAMPTA*, 2013, pp. 1–8.

[13] Z. Yang, L. Xie, and C. Zhang, "Variational Bayesian algorithm for quantized compressed sensing," *IEEE Trans. Signal Process.*, vol. 61, no. 11, pp. 2815–2824, Jun. 2013.

[14] L. Jacques, D. K. Hammond, and J. M. Fadili, "Dequantizing compressed sensing: When oversampling and non-Gaussian constraints combine," *IEEE Trans. Inf. Theory*, vol. 57, no. 1, pp. 559–571, Jan. 2011.

[15] V. Cambareri, M. Mangia, F. Pareschi, R. Rovatti, and G. Setti, "Low-complexity multiclass encryption by compressed sensing," *IEEE Trans. Signal Process.*, vol. 63, no. 9, pp. 2183–2195, May 2015.

[16] J. Haboba, M. Mangia, F. Pareschi, R. Rovatti, and G. Setti, "A pragmatic look at some compressive sensing architectures with saturation and quantization," *IEEE J. Emerg. Sel. Topics Circuits Syst.*, vol. 2, no. 3, pp. 443–459, Sep. 2012.

[17] A. Wang, W. Xu, Z. Jin, and F. Gong, "Quantization effects in an analog-to-information front end in EEG telemonitoring," *IEEE Trans. Circuits Syst. II, Exp. Briefs*, vol. 62, no. 2, pp. 104–108, Feb. 2015.

[18] A. Wang, Z. Jin, C. Song, and W. Xu, "Adaptive compressed sensing architecture in wireless brain-computer interface," in *Proc. 52nd ACM/EDAC/IEEE Annu. Design Autom. Conf.*, Jun. 2015, pp. 1–6.

[19] Z. Zhang, Z. Pi, and B. Liu, "TROIKA: A general framework for heart rate monitoring using wrist-type photoplethysmographic signals during intensive physical exercise," *IEEE Trans. Biomed. Eng.*, vol. 62, no. 2, pp. 522–531, Feb. 2015.

[20] R. Prasad, C. R. Murthy, and B. D. Rao, "Nested sparse Bayesian learning for block-sparse signals with intra-block correlation," in *Proc. IEEE Int. Conf. Acoust., Speech Signal Process. (ICASSP)*, May 2014, pp. 7183–7187.

[21] Z. Zhang and B. D. Rao, "Sparse signal recovery with temporally correlated source vectors using sparse Bayesian learning," *IEEE J. Sel. Topics Signal Process.*, vol. 5, no. 5, pp. 912–926, Sep. 2011.

[22] S. D. Babacan, S. Nakajima, and M. N. Do, "Bayesian group-sparse modeling and variational inference," *IEEE Trans. Signal Process.*, vol. 62, no. 11, pp. 2906–2921, Jun. 2014.

[23] A. N. Akansu and M. U. Torun, "Toeplitz approximation to empirical correlation matrix of asset returns: A signal processing perspective," *IEEE J. Sel. Topics Signal Process.*, vol. 6, no. 4, pp. 319–326, Aug. 2012.

[24] G. Strang, "The discrete cosine transform," *SIAM Rev.*, vol. 41, no. 1, pp. 135–147, 1999.

[25] B. Liu, Z. Zhang, H. Fan, and Q. Fu, "Compression via compressive sensing: A low-power framework for the telemonitoring of multi-channel physiological signals," in *Proc. IEEE Int. Conf. Bioinform. Biomed. (BIBM)*, Dec. 2013, pp. 9–12.

[26] Z. Wang and A. C. Bovik, "Mean squared error: Love it or leave it? A new look at signal fidelity measures," *IEEE Signal Process. Mag.*, vol. 26, no. 1, pp. 98–117, Jan. 2009.

[27] A. Zymnis, S. Boyd, and E. J. Candès, "Compressed sensing with quantized measurements," *IEEE Signal Process. Lett.*, vol. 17, no. 2, pp. 149–152, Feb. 2010.

[28] Z. Zhang, B. D. Rao, and T. P. Jung, "Compressed sensing for energy-efficient wireless telemonitoring: Challenges and opportunities," in *Proc. Asilomar Conf. Signals, Syst. Comput. (AsiloMar)*, Nov. 2013, pp. 80–85.

Benyuan Liu received the M.S. and Ph.D. degrees in information and communication engineering from the National University of Defense Technology, in 2009 and 2015, respectively. He is currently a Lecturer with the Fourth Military Medical University. His research activities focus on electrical impedance tomography and inverse problems.

Zhilin Zhang, photograph and biography not available at the time of publication.